Path Entanglement of Continuous-Variable Quantum Microwaves

E. P. Menzel,[1,2,*] R. Di Candia,[3] F. Deppe,[1,2] P. Eder,[1,2] L. Zhong,[1,2] M. Ihmig,[4] M. Haeberlein,[1,2] A. Baust,[1,2] E. Hoffmann,[1,2] D. Ballester,[5,3] K. Inomata,[6] T. Yamamoto,[7,6] Y. Nakamura,[8,6] E. Solano,[3,9] A. Marx,[1] and R. Gross[1,2]

[1]*Walther-Meißner-Institut, Bayerische Akademie der Wissenschaften, D-85748 Garching, Germany*
[2]*Physik-Department, Technische Universität München, D-85748 Garching, Germany*
[3]*Departamento de Química Física, Universidad del País Vasco UPV/EHU, Apartado 644, 48080 Bilbao, Spain*
[4]*Lehrstuhl für Integrierte Systeme, Technische Universität München, D-80333 München, Germany*
[5]*Department of Physics and Astronomy, University College London, London WC1E 6BT, United Kingdom*
[6]*RIKEN Advanced Science Institute, Wako, Saitama 351-0198, Japan*
[7]*NEC Smart Energy Research Laboratories, Tsukuba, Ibaraki 305-8501, Japan*
[8]*Research Center for Advanced Science and Technology (RCAST), The University of Tokyo, Komaba, Meguro-ku, Tokyo 153-8904, Japan*
[9]*IKERBASQUE, Basque Foundation for Science, Alameda Urquijo 36, 48011 Bilbao, Spain*

(Received 8 October 2012; published 18 December 2012)

Path entanglement constitutes an essential resource in quantum information and communication protocols. Here, we demonstrate frequency-degenerate entanglement between continuous-variable quantum microwaves propagating along two spatially separated paths. We combine a squeezed and a vacuum state using a microwave beam splitter. Via correlation measurements, we detect and quantify the path entanglement contained in the beam splitter output state. Our experiments open the avenue to quantum teleportation, quantum communication, or quantum radar with continuous variables at microwave frequencies.

DOI: 10.1103/PhysRevLett.109.250502 PACS numbers: 03.67.Bg, 03.65.Ud, 42.50.Dv, 85.25.−j

Fascinatingly, quantum mechanics allows for a compound system to have a common description while, at the same time, no individual states can be ascribed to its subsystems [1]. The presence of entanglement between spatially separated systems is a necessary condition for what Einstein called "spooky action at a distance" [2]: the contradiction between quantum mechanics and local realism [1,3]. Furthermore, entanglement is at the heart of quantum communication and information processing technologies, which promise significant performance gains over classical protocols [1,4,5]. Consequently, entanglement has been extensively explored in atomic physics and quantum optics [4–6]. In these investigations, optical frequencies were preferred over microwaves because the higher photon energies facilitate practical applications. However, since the late 1990s, microwave technology has evolved rapidly in both industry and science. For one thing, classical microwave fields have become an indispensable tool in mobile communication. For another, a promising direction towards scalable quantum information processing has appeared with the advent of superconducting microwave quantum circuits [7–9]. Despite some decoherence issues, these systems provide unprecedented light-matter coupling strengths due to their large effective dipole moments and field enhancement effects [10,11]. As a consequence, standing-wave fields in transmission line resonators were shown to act as a short-range quantum bus between superconducting qubits [12,13] and various gates were implemented [12–16]. For microwave quantum communication, however, propagating fields are required. As a first step in this direction, early experiments demonstrated tomography of weak thermal states [17], coherent states [18], and single photons [19]. Next, continuous-variable states generated by Josephson parametric devices were reconstructed [20]. Very recently, such devices have permitted to investigate two-mode squeezing [21,22] and frequency nondegenerate path entanglement [23]. An important aspect of these experiments is the understanding they provide regarding entanglement. In order to be a resource in quantum communication protocols, it must occur between spatially separated subsystems [1]. Furthermore, a strict proof of entanglement requires the entangler and the detector to be based on independent experimental techniques. In this work, we make a significant step beyond previous efforts and demonstrate frequency-degenerate path entanglement in the microwave regime. We respect both criteria mentioned above by directly measuring the correlations between two different propagation paths. Our experiments follow the spirit of the quantum-optical realization [6] of the original Einstein-Podolsky-Rosen (EPR) paradox [3]. As shown in Fig. 1, we combine a vacuum and a squeezed vacuum state in a hybrid ring microwave beam splitter [24] acting as an entangling device. Its two output ports hold a continuous-variable state which is frequency degenerate and entangled with respect to the two propagation paths. Along these paths, the entanglement can be conveniently distributed to two parties requiring it for any suitable quantum communication protocol. In our experiments, we first reconstruct the squeezed *input* state by means of dual-path tomography [18], which assumes knowledge of the beam splitter relations. Next, we reconstruct the moments of the *output* state

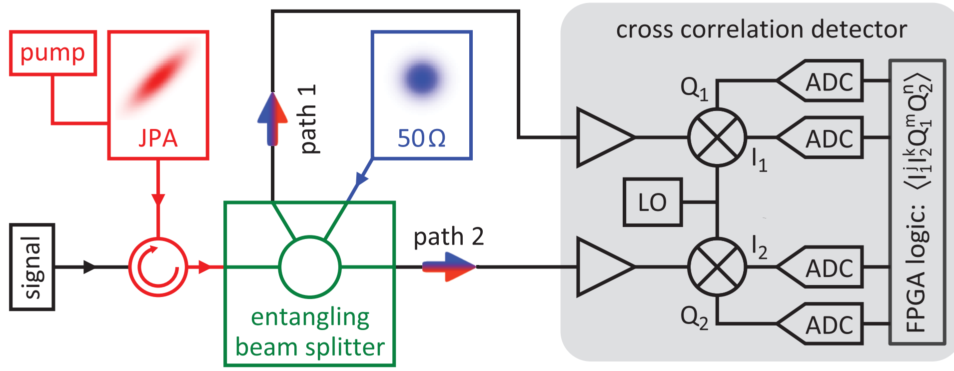

FIG. 1 (color). Layout of the experiment. The JPA is operated in reflection using a circulator (red circle). A 180°-hybrid ring microwave beam splitter (green) acts as entangling device. The vacuum state (blue) is realized by a 50 Ω load at 40 mK. The signal can be a thermal state or a (displaced) vacuum and becomes squeezed by the JPA when the pump is on. The blue-and-red arrows denote the output state, which can be path-entangled. The cross correlation detector consists of two noisy amplification (triangular symbols) and analog down-conversion (circles with crosses) paths. LO denotes the common local oscillator which is detuned by 11 MHz. Analog-to-digital converters (ADCs) digitize the in-phase ($I_{1,2}$) and quadrature ($Q_{1,2}$) components of the output state. After digital down-conversion and filtering, the averaged moments $\langle I_1^j I_2^k Q_1^m Q_2^n \rangle$ are computed in real time using an FPGA logic.

after the beam splitter by treating the latter as a black box and calibrating against a known state [25]. In this reference-state method [26], we only assume that independent vacuum states are produced in each output path when vacuum is incident at both input ports. From the moments reconstructed in this way, we build a witness matrix which proves the existence of path entanglement independently of the detailed nature of our output state [27]. Since in practice the data show that our states are Gaussian, we finally quantify the degree of entanglement by means of the negativity [28]. The result of this analysis agrees with what we expect for our squeezed input state. We note here that for bipartite single-mode Gaussian entanglement, as it is relevant in our case, entanglement implies nonlocality [1,5]. All in all, our results show that we have realized the main building block for microwave quantum teleportation and communication protocols.

The generation of the input states for the beam splitter is straightforward. The vacuum is realized with a commercial 50 Ω termination at 40 mK acting as a broadband blackbody emitter [17]. The squeezed state is produced using a particular superconducting circuit, the flux-driven Josephson parametric amplifier (JPA) [29]. In this device two Josephson junctions form a nonlinearity which can be modulated ("pumped") at gigahertz frequencies to achieve a parametric effect. The JPA box is stabilized to 50 mK. A thermal state emitted by an attenuator, whose temperature can be varied from 50 to 800 mK, can be fed into the JPA. Our cross correlation detector is based on the insight that for microwave signals off-the-shelf high-gain low-noise linear amplifiers are available rather than efficient single photon counters. We connect one amplification path to each output port of the beam splitter. At room temperature we record the in-phase and quadrature components, $I_{1,2}$ and $Q_{1,2}$ of the amplified signals. The averaged moments $\langle I_1^j I_2^k Q_1^m Q_2^n \rangle$ are computed for $j + k + m + n \leq 4$ and j, k, m, $n \in \mathbb{N}_0$ in real time using a field programmable gate array (FPGA) logic. We typically average over $7.7 \times 10^8 - 5.7 \times 10^9$ samples and all subsequently given error bars are based on this statistics. Further details can be found in the Supplemental Material [26].

As a first test of our setup, we perform dual-path reconstructions of the Wigner function for known input states. Here, we exploit the fact that the noise contributions of the two amplification paths are independent, while the split signals are correlated [18,26]. We reconstruct vacuum fluctuations and coherent states (displaced vacuum), both at a frequency $f_0 = 5.637$ GHz. Because of the narrow measurement bandwidth of 978 kHz, we approximate the vacuum and thermal states as single-mode fields. The results shown in Fig. 2(a) exhibit a very good phase control for the coherent state. In addition, we find a small thermal contribution of 0.097 ± 0.007 photons above the vacuum level which can be due to a small thermal population or other experimental imperfections. In the next step, we generate a squeezed state by pumping the JPA at $2f_0$. For a signal gain of 10 dB and a phase of 45°, the reconstructed Wigner function is shown in Fig. 2(b). An analysis of the reconstructed signal moments reveals that, at the input of the beam splitter, the state generated by the JPA is squeezed by 4.9 ± 0.2 dB below the vacuum level and contains 8.72 ± 0.05 photons. Furthermore, the product of the standard deviation of the squeezed quadrature with that of its orthogonal, enlarged one, is 3.45 ± 0.07 times larger than the variance of the ideal vacuum. In other words, we can model the state as one created by an ideal squeezer acting on an effective thermal field with 1.22 ± 0.04 photons. This thermal field contains the combined effects of losses and the small thermal population found in the experimental vacuum. Again, we notice good control of the phase. It is noteworthy to mention that the amount of squeezing quoted above is mainly limited by cable losses and not by the JPA itself.

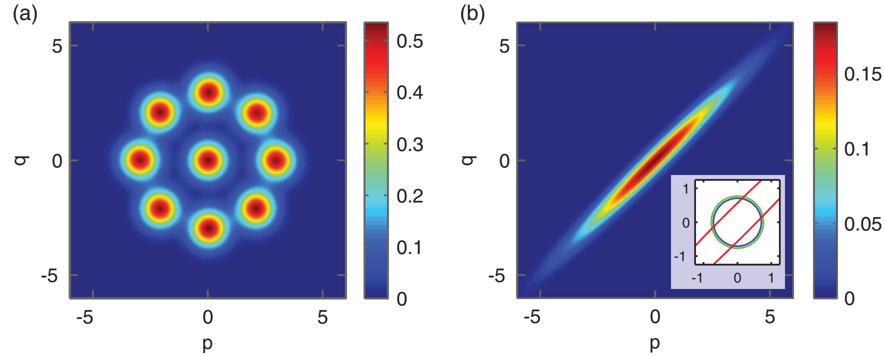

FIG. 2 (color). Dual-path reconstruction of various states incident at the "squeezed state input port" of the beam splitter. p and q are dimensionless variables spanning the phase space. (a) JPA pump off. Reconstruction of the vacuum and of displaced vacuum states (coherent states, 8.80 ± 0.01 photons, eight different phase values). All nine Wigner functions are superposed. (b) JPA pump on. Squeezed state for 10 dB JPA signal gain at 45°. Inset: $1/e$ contours of the ideal vacuum (blue), the experimental vacuum (green) displayed in panel (a), and the squeezed state (red).

After characterizing the input fields of the beam splitter, we now turn to its outputs. With the reference-state method, we build an entanglement witness matrix from the reconstructed moments. Our witness reliably distinguishes between "separable outputs" for the vacuum state and "path entangled outputs" for the squeezed state input. Next, we analyze the third and fourth order cumulants and find them to be small for JPA signal gains up to 10 dB. Since this is a strong indication for Gaussian states, we explore the path entanglement generated in our setup quantitatively via the negativity $\mathcal{N}_{\text{out}}$. For positive values, $\mathcal{N}_{\text{out}}$ describes the degree of entanglement produced between the beam splitter output paths [26]. In the limit of low JPA signal gain, Fig. 3(a) shows how $\mathcal{N}_{\text{out}}$ becomes suppressed when sending more and more thermal photons into the JPA. At some point, the JPA cannot squeeze the incoming field below the vacuum anymore and the output state is no longer entangled. For a constant temperature, Fig. 3(b) shows how $\mathcal{N}_{\text{out}}$ increases with increasing signal gain from zero to a value $\mathcal{N}_{\text{out,max}} = 0.55 \pm 0.04$ at 10 dB signal gain. This behavior is in good agreement with the negativity $\mathcal{N}_{\text{calc}}$ calculated from the dual-path reconstructed input state. Again, we observe a suppression for large thermal fields sent into the JPA. Our results confirm the expectation [30] that the degree of squeezing at the beam splitter input determines the amount of entanglement generated between the output paths. However, since $\mathcal{N}_{\text{calc}}$ is generally slightly lower than $\mathcal{N}_{\text{out}}$, we conclude that either the dual-path reconstruction underestimates the squeezing at the beam splitter input or the reference-state method ignores a small amount of spurious classical correlations between the two paths. Both effects are consistent with the data shown in Fig. 3(a), where at constant signal gain, the curve measured with the reference-state method at the beam splitter output converges for high temperatures to that calculated from the dual-path reconstructed input state. We finally note that the path-entangled state is expected to be a two-mode squeezed state with two additional local squeezing operations applied to it [30]. Since local operations do not change the amount of

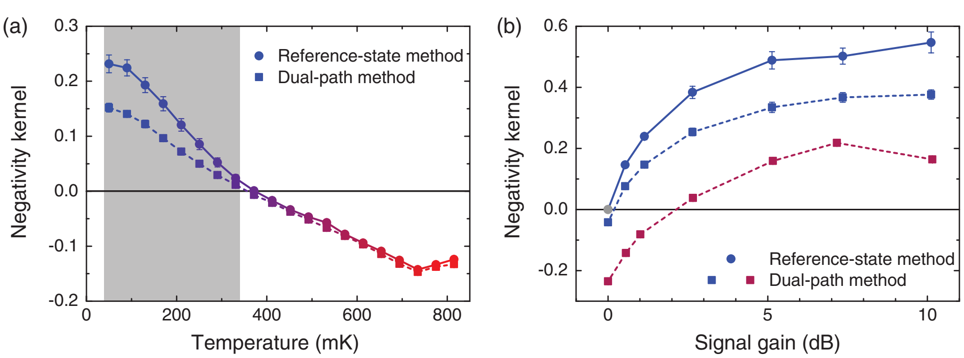

FIG. 3 (color). Quantitative analysis of the path entanglement generated in our experiments. The negativities $\mathcal{N}_{\text{out}}$, $\mathcal{N}_{\text{calc}}$ are the maxima of the corresponding negativity kernels $\tilde{\mathcal{N}}_{\text{out}}$, $\tilde{\mathcal{N}}_{\text{calc}}$, and 0. Circular symbols: $\tilde{\mathcal{N}}_{\text{out}}$ data at the beam splitter output. Square symbols: $\tilde{\mathcal{N}}_{\text{calc}}$ calculated from the reconstructed input state. The lines are guides to the eye. (a) Negativity kernel versus attenuator temperature (color code) at 1 dB signal gain. For the data points in the shaded area, the witness matrix [27] confirms entanglement. (b) Negativity kernel versus the JPA signal gain. The blue (red) curves are recorded at 50 mK (573 mK). Grey point: Negativity of the reference state, assumed to be zero.

entanglement, the negativity $\mathcal{N}_{\text{out,max}} = 0.55 \pm 0.04$ implies that the two-mode squeezed state before the two local operations would have a variance squeezed by 3.2 ± 0.2 dB below that of the two-mode vacuum.

In summary, we present clear evidence for path entanglement generated by combining two frequency-degenerate continuous-variable microwave fields, the vacuum and the squeezed vacuum, in a beam splitter. For an input state squeezed 4.9 ± 0.2 dB below the vacuum, we observe a maximum negativity $\mathcal{N}_{\text{out,max}} = 0.55 \pm 0.04$ at 10 dB JPA signal gain. Our experiments bring the exciting quantum physics of entangled propagating electromagnetic fields to the technologically highly attractive microwave domain. In this way, they open up new and exciting perspectives towards microwave quantum teleportation, quantum communication, and quantum radar [31].

The authors thank C. Probst, K. Neumaier, and K. Uhlig for support on cryogenic technologies and C. Eichler for discussions. We acknowledge support from the Deutsche Forschungsgemeinschaft via the Sonderforschungsbereich 631, the German excellence initiative via the "Nanosystems Initiative Munich" (NIM), from the EU projects SOLID, CCQED and PROMISCE, from MEXT Kakenhi "Quantum Cybernetics", the JSPS through its FIRST Program, the Project for Developing Innovation Systems of MEXT, the NICT Commissioned Research, EPSRC EP/H050434/1, Basque Government IT472-10, and Spanish MICINN FIS2009-12773-C02-01.

*Edwin.Menzel@wmi.badw-muenchen.de

[1] R. Horodecki, P. Horodecki, M. Horodecki, and K. Horodecki, Rev. Mod. Phys. **81**, 865 (2009).
[2] M. Born, *The Born-Einstein Letters* (Walker and Company, New York, 1971).
[3] A. Einstein, B. Podolsky, and N. Rosen, Phys. Rev. **47**, 777 (1935).
[4] J. Raimond, M. Brune, and S. Haroche, Rev. Mod. Phys. **73**, 565 (2001).
[5] S.L. Braunstein and P. van Loock, Rev. Mod. Phys. **77**, 513 (2005).
[6] Z. Y. Ou, S. F. Pereira, H. J. Kimble, and K. C. Peng, Phys. Rev. Lett. **68**, 3663 (1992).
[7] R.J. Schoelkopf and S.M. Girvin, Nature (London) **451**, 664 (2008).
[8] J. Clarke and F.K. Wilhelm, Nature (London) **453**, 1031 (2008).
[9] M. Mariantoni, H. Wang, T. Yamamoto, M. Neeley, R.C. Bialczak, Y. Chen, M. Lenander, E. Lucero, A.D. O'Connell, D. Sank, M. Weides, J. Wenner, Y. Yin, J. Zhao, A.N. Korotkov, A.N. Cleland, and J.M. Martinis, Science **334**, 61 (2011).
[10] A. Wallraff, D.I. Schuster, A. Blais, L. Frunzio, R.-S. Huang, J. Majer, S. Kumar, S.M. Girvin, and R.J. Schoelkopf, Nature (London) **431**, 162 (2004).
[11] T. Niemczyk, F. Deppe, H. Huebl, E.P. Menzel, F. Hocke, M.J. Schwarz, J.J. Garcia-Ripoll, D. Zueco, T. Hümmer, E. Solano, A. Marx, and R. Gross, Nat. Phys. **6**, 772 (2010).
[12] J. Majer, J.M. Chow, J.M. Gambetta, J. Koch, B.R. Johnson, J.A. Schreier, L. Frunzio, D.I. Schuster, A.A. Houck, A. Wallraff, A. Blais, M.H. Devoret, S.M. Girvin, and R.J. Schoelkopf, Nature (London) **449**, 443 (2007).
[13] M.A. Sillanpää, J.I. Park, and R.W. Simmonds, Nature (London) **449**, 438 (2007).
[14] T. Yamamoto, Yu. A. Pashkin, O. Astafiev, Y. Nakamura, and J.S. Tsai, Nature (London) **425**, 941 (2003).
[15] J.H. Plantenberg, P.C. de Groot, C.J.P. M. Harmans, and J.E. Mooij, Nature (London) **447**, 836 (2007).
[16] M. Ansmann, H. Wang, R.C. Bialczak, M. Hofheinz, E. Lucero, M. Neeley, A.D. O'Connell, D. Sank, M. Weides, J. Wenner, A.N. Cleland, and J.M. Martinis, Nature **461**, 504 (2009).
[17] M. Mariantoni, E.P. Menzel, F. Deppe, M.Á. Araque Caballero, A. Baust, T. Niemczyk, E. Hoffmann, E. Solano, A. Marx, and R. Gross, Phys. Rev. Lett. **105**, 133601 (2010).
[18] E.P. Menzel, F. Deppe, M. Mariantoni, M.Á. Araque Caballero, A. Baust, T. Niemczyk, E. Hoffmann, A. Marx, E. Solano, and R. Gross, Phys. Rev. Lett. **105**, 100401 (2010).
[19] D. Bozyigit, C. Lang, L. Steffen, J.M. Fink, C. Eichler, M. Baur, R. Bianchetti, P.J. Leek, S. Filipp, M.P. da Silva, A. Blais, and A. Wallraff, Nat. Phys. **7**, 154 (2011).
[20] F. Mallet, M.A. Castellanos-Beltran, H.S. Ku, S. Glancy, E. Knill, K.D. Irwin, G.C. Hilton, L.R. Vale, and K.W. Lehnert, Phys. Rev. Lett. **106**, 220502 (2011).
[21] C. Eichler, D. Bozyigit, C. Lang, M. Baur, L. Steffen, J.M. Fink, S. Filipp, and A. Wallraff, Phys. Rev. Lett. **107**, 113601 (2011).
[22] C.M. Wilson, G. Johansson, A. Pourkabirian, M. Simoen, J.R. Johansson, T. Duty, F. Nori, and P. Delsing, Nature **479**, 376 (2011).
[23] E. Flurin, N. Roch, F. Mallet, M.H. Devoret, and B. Huard, Phys. Rev. Lett. **109**, 183901 (2012).
[24] E. Hoffmann, F. Deppe, T. Niemczyk, T. Wirth, E.P. Menzel, G. Wild, H. Huebl, M. Mariantoni, T. Weißl, A. Lukashenko, A.P. Zhuravel, A.V. Ustinov, A. Marx, and R. Gross, Appl. Phys. Lett. **97**, 222508 (2010).
[25] C. Eichler, D. Bozyigit, C. Lang, L. Steffen, J. Fink, and A. Wallraff, Phys. Rev. Lett. **106**, 220503 (2011).
[26] See Supplemental Material at http://link.aps.org/supplemental/10.1103/PhysRevLett.109.250502 for details on experimental and theoretical methods.
[27] E. Shchukin and W. Vogel, Phys. Rev. Lett. **95**, 230502 (2005).
[28] G. Adesso and F. Illuminati, Phys. Rev. A **72**, 032334 (2005).
[29] T. Yamamoto, K. Inomata, M. Watanabe, K. Matsuba, T. Miyazaki, W.D. Oliver, Y. Nakamura, and J.S. Tsai, Appl. Phys. Lett. **93**, 042510 (2008).
[30] M.S. Kim, W. Son, V. Bužek, and P.L. Knight, Phys. Rev. A **65**, 032323 (2002).
[31] M. Lanzagorta, in *Quantum Radar*, Synthesis Lectures on Quantum Computing Vol. 5, edited by M. Lanzagorta and J. Uhlmann (Morgan & Claypool Publishers, 2012).